



# HHS Public Access

Author manuscript

*Anal Chem.* Author manuscript; available in PMC 2017 August 14.

Published in final edited form as:

*Anal Chem.* 2017 June 20; 89(12): 6551–6558. doi:10.1021/acs.analchem.7b00691.

## Rapid Elemental Analysis of Aerosols Using Atmospheric Glow Discharge Optical Emission Spectroscopy

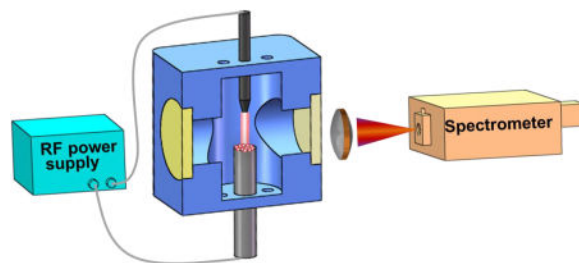
Lina Zheng and Pramod Kulkarni\*

Centers for Disease Control and Prevention, National Institute for Occupational Safety and Health, Cincinnati, Ohio 45226, United States

### Abstract

A new, low-cost approach based on the application of atmospheric radio frequency glow discharge (rf-GD) optical emission spectroscopy (OES) has been developed for near real-time measurement of multielemental concentration in airborne particulate matter. This method involves deposition of aerosol particles on the tip of a grounded electrode of a coaxial microelectrode system, followed by ablation, atomization and excitation of the particulate matter using the rf-GD. The resulting atomic emissions were recorded using a spectrometer for elemental identification and quantification. The glow discharge plasma was characterized by measuring spatially resolved gas temperatures (378 – 1438 K) and electron densities ( $2 - 5 \times 10^{14} \text{ cm}^{-3}$ ). Spatial analysis of the spectral features showed that the excitation of the analyte occurred in the region near the collection electrode. The temporal analysis of spectral features in the rf-GD showed that the collected particles were continuously ablated; the time for complete ablation of 193 ng of sucrose particles was found to be approximately 2 s. The system was calibrated using 100 nm particles containing C, Cd, Mn, and Na, respectively. Our method provides limits of detection in the range of 0.055 – 1.0 ng, and a measurement reproducibility of 5 – 28%. This study demonstrates that the rf-GD can be an excellent excitation source for the development of low-cost hand-held sensors for elemental measurement of aerosols.

### Graphical Abstract



\* Author to whom correspondence should be addressed to: Phone: (513) 841-4300; Fax: (513) 841-4545; PSKulkarni@cdc.gov.

#### ASSOCIATED CONTENT

##### Supporting Information

Supporting information is available free of charge on the ACS Publications website: i) voltage and current characteristics of the rf-GD system; ii) calculation of glow discharge gas temperature and electron density

Airborne particles effect the global climate, air quality, and human health.<sup>1</sup> In particular, long-term inhalation of toxic particulate matter could pose a significant health risk to those who are routinely exposed to airborne particles, such as in workplaces. Measurement of exposure to metals is essential to environmental and occupational health studies. Existing elemental analysis methods, such as atomic absorption spectroscopy (AAS), X-ray fluorescence spectroscopy (XRFS), inductively coupled plasma atomic emission spectroscopy (ICP-AES) and mass spectroscopy (ICP-MS), are effective for chemical analysis of particulate matter and have been widely used for routine monitoring of personal exposure because of their high sensitivity and accuracy.<sup>2,3</sup> These methods require particle collection on filters over several hours, followed by subsequent laboratory analysis, and are labor- and time-intensive. Low-cost, field portable, near real-time instruments for chemical analysis of aerosol are desired to address these limitations.

Several plasma-based techniques have been used for elemental analysis of aerosols, which have employed excitation sources such as spark microplasma,<sup>4-7</sup> laser-induced microplasma,<sup>8-11</sup> and microwave induced plasma.<sup>12,13</sup> However, the excitation sources used in these methods can be bulky and costly, making them unsuitable for hand-held, low-cost monitors for aerosol elemental analysis. In this context, the glow-discharge excitation sources offer attractive alternatives for development of low-cost aerosol instruments. Glow discharge, as an excitation source for elemental determination, has unique advantages with respect to development of hand-held sensors such as low cost, low power consumption, and analytical versatility.<sup>14</sup> Glow discharge optical emission spectroscopy (GD-OES) and glow discharge mass spectroscopy (GD-MS) have been applied to the bulk elemental analysis of inorganic solid samples<sup>15,16</sup> and quantitative depth profile analysis.<sup>17</sup> In a glow discharge system, the samples function as the cathode, and are continuously eroded by bombardment of ions and neutral species from the plasma. The free atoms ejected from the samples diffuse into the plasma plume, where they are excited through collisions with electrons, metastable gas atoms, and ions, leading to element-specific optical emission.<sup>18,19</sup> In 1993, Cserfalvi and Meze introduced an electrolyte cathode discharge (ELCAD) for elemental analysis of solutions.<sup>20</sup> Since then, solution-cathode glow discharge (SCGD) and liquid sampling-atmospheric pressure glow discharge (LS-APGD) methods have been developed for elemental analysis of solutions.<sup>21-23</sup> These techniques can offer similar detection limits (tens of ppbs) as ICP-AES, but have the advantage of much lower cost and power consumption.<sup>22,24</sup> GD-OES and GD-MS have also been applied to aerosol analysis. Marcus et al. conducted elemental analysis of aerosols by a direct injection of particles into a low-pressure glow discharge plasma using an aerodynamic lens system, and obtained limits of detection (LOD) on the order of tens of nanograms.<sup>25</sup> However, the aerodynamic lens method required use of large turbo pumps to create particle beams for direct injection into GD, making the technique unsuitable for hand-held instrumentation.

The objective of this study was to develop a near real-time method for aerosol elemental analysis using a low-cost atmospheric radio frequency glow discharge (rf-GD) excitation source. A corona-based microconcentration method<sup>26</sup> was used for microscopic collection of airborne particles, followed by elemental analysis using rf-GD-OES. A methodology was developed for automated and semi-continuous analysis of aerosol. The spectral features and signal stability of this rf-GD-OES aerosol analysis system were investigated. The glow

discharge plasma was characterized by measuring its gas temperature and electron density using spectroscopic methods. Analytical figures of merit were determined for select elements of interest (C, Cd, Mn, and Na), and are compared with other microplasma spectroscopy methods.

## EXPERIMENTAL SECTION

### Experimental Setup

A schematic diagram of the experimental setup is shown in Figure 1. The major components included: (i) an aerosol generation system, (ii) an aerosol collection system, and (iii) a rf-GD-OES system. The aerosol generation and collection systems were similar to those described in previously published studies.<sup>4,9</sup>

### Aerosol Generation

Test aerosols were generated using a pneumatic atomizer (Model 3080, TSI Inc., Shoreview, MN, USA) to atomize solutions containing analytes and then passed through a diffusion dryer. A differential mobility analyzer (DMA; model 3080, TSI Inc., Shoreview, MN, USA), a neutralizer, and an electrostatic precipitator were used to obtain near-monodisperse uncharged particles for calibration purpose. In this study, 100 nm diameter particles classified by DMA were used for all calibration studies. Table 1 shows materials containing C, Na, Cd, and Mn used for calibration. Stock standard solutions, containing desired elements, were diluted using ultrafiltered deionized water to obtain solutions, ranging from 100 to 1000  $\mu\text{g mL}^{-1}$  depending on the analyte.

### Aerosol Collection

The test aerosol particles were then introduced into a corona aerosol microconcentrator (CAM). Detailed description of design and performance of CAM was provided elsewhere.<sup>26</sup> Briefly, the CAM consisted of two coaxial electrodes with an interelectrode distance of 4 mm. A high positive potential ( $\sim 5$  kV) was applied to the corona electrode through a DC power supply (Bertran S-230, Spellman Corp., Hauppauge, NY, USA). The corona electrode, made of tungsten, had a shaft diameter of 200  $\mu\text{m}$  and a sharp tip with an approximate radius of 50  $\mu\text{m}$ . The ground electrode, made of platinum, was 500  $\mu\text{m}$  in diameter, and had a relatively flat tip to provide a planar surface for particle deposition. The aerosol particles entering the CAM were collected on the tip of the ground electrode. The sidewalls of the ground electrode were covered with a high dielectric strength sheath [polyether ether ketone (PEEK), 1.58 mm outer diameter and 0.40 mm wall thickness; McMaster-Carr, Princeton, NJ, USA]. The flat tip of the ground electrode was bare to allow aerosol sample collection. This same electrode system was also used to produce the radio-frequency glow discharge at the tip of the collection electrode. A constant flow rate of 1.5 L  $\text{min}^{-1}$  of aerosol was maintained through the CAM and was driven by the internal pump of the condensation particle counter (CPC; model 3022A, TSI Inc., Shoreview, MN, USA). The overall flow scheme was controlled using a mass flow controller (MFC; model 247 C, MKS Instruments, Inc., Andover, MA, USA).

## rf-GD-OES System

Glow discharge was generated in the CAM in an argon atmosphere using a radio frequency power supply (Information Unlimited, Amherst, NH, Model PVM500; with a maximum output voltage of 1.6 kV and a frequency of 27.6 kHz). Similar power supplies have been successfully used for generating microplasmas for elemental analysis in previous studies.<sup>27–29</sup> The power supply is relatively inexpensive, very compact, light-weight, and consumes low power, which makes it suitable for hand-held instrumentation. The measured voltage and current characteristics for the interelectrode system in our CAM are shown in Figure S-1 in the Supplemental Information (SI). After the particle collection, pre-purified argon gas was introduced into the chamber at a constant flow rate of 0.9 L min<sup>-1</sup> at atmospheric pressure. Once the glow discharge was initiated, the collected particulate matter on the ground electrode surface was ablated over few seconds (the time required for complete ablation of the sample depends on the particle mass). The glow discharge in the interelectrode gap was focused onto the spectrograph (Iso-Plane SCT320, Princeton Instrument Inc., Trenton, NJ, USA) using an UV-grade plano-convex lens ( $f=50$  mm). The spectrograph was coupled with a gated intensified charge-coupled device (ICCD; iStar 334T, Andor Technology, South Windsor, CT, USA), which allowed recording of space- and time-resolved emission spectra from the glow discharge during the particulate sample ablation. The multi-track mode of the ICCD was used to record the space-resolved spectra, and the kinetic mode was used to record the time-resolved spectra. The wavelength calibration was achieved using an Hg-Ar lamp (Ocean Optics Inc., Dunedin, FL, USA). Triggering of the spectrograph, RF power supply and data acquisition were controlled through the built-in digital delay generator in the ICCD.

## Calibration Procedure

The calibration procedure consisted of the following steps: (i) generation of test aerosols, (ii) collection of particles on the flat tip of the ground electrode for predetermined amount of time, (iii) ablation of the collected particles by glow discharge, (iv) recording of the time-resolved emission spectra during glow discharge, (v) calculation of the emission signal for analyte of interest for each spectrum, (vi) calculation of the time-integrated signal intensity for the analyte of interest, and (vii) construction of the calibration curve by plotting the integrated signal intensity as a function of analyte mass. Particulate mass deposited on the electrode for the known diameter of particles is given by,

$$m_p = \eta C_m Q_f t_c \rho_p \frac{\pi}{6} d_v^3 \quad (1)$$

where  $\eta$  is the capture efficiency of particles,  $C_m$  is the particle concentration flowing into the chamber,  $Q_f$  is the aerosol volumetric flow rate,  $t_c$  is the particle collection time,  $\rho_p$  is the particle material density, and  $d_v$  is the volume equivalent particle diameter. Assuming the particles are spherical, the volume equivalent diameter is equal to the electrical mobility diameter. Particle capture efficiency was calculated by measuring the particle number concentration downstream of the collection unit using a CPC, with or without the presence of the electric field across the electrodes ( $N_{\text{out}}^{\text{HV}}$  and  $N_{\text{out}}^{V=0}$ ):

$$\eta = \frac{N_{\text{out}}^{V=0} - N_{\text{out}}^{\text{HV}}}{N_{\text{out}}^{V=0}} \quad (2)$$

Particulate elemental mass loadings on the ground electrode of 1 to 100 ng were achieved by varying the collection time. For each mass loading, three replicate measurements were performed and the final calibration curve was constructed by averaging over the three independent sets of measurements. The atomic emission from glow discharge was recorded kinetically with a gate width of 500 ms during a total cumulative period of 10 seconds for individual measurement. The total emission signal from the target analyte with known mass was obtained by adding time-dependent signal over the life of the glow discharge. The calibration curve was constructed by plotting the total signal intensity as a function of mass loaded on the collection electrode.

## RESULTS AND DISCUSSION

### Plasma gas temperature and electron density

We measured the gas temperature of the glow discharge using the van der Waals broadening of Ar I emission line. The method for the gas temperature calculation is described in Section S.2 of the Supplemental Information (SI) available online. Figure 2(a) shows the gas temperature as a function of interelectrode distance on the x-axis. Higher gas temperatures were observed in the region close to the electrode surface. This was consistent with earlier studies on the DC glow discharge, which show that the gas temperature is higher at the cathode surface and decreases with the distance away from the cathode.<sup>30–32</sup> This was attributed to the increasing collisions between gas molecules and electrons emitted from the cathode surface. In our rf-GD system, the two electrodes alternated between cathode and anode, leading to a higher temperature in the region close to both electrodes. The gas temperature of the rf-GD in our system is in the range of 378 – 1438 K, which was similar to those reported in the literature.<sup>33,34</sup> Different techniques have been employed for measuring the gas temperature of glow discharge, which include filtered Rayleigh scattering,<sup>35</sup> Doppler broadening,<sup>30</sup> heat transport equilibrium,<sup>32</sup> and van der Waals broadening.<sup>33</sup> The gas temperature depends on the type of the glow discharge, carrier/working gas composition, gas flow rate, and the electrical characteristics of the discharge. The gas temperature of DC glow discharge has been reported to be in the range 700–900 K by Obradovic and Kuraica,<sup>30</sup> 300–800 K by Yalin et al.,<sup>35</sup> and 300–360 K by Revel et al.<sup>32</sup> The gas temperature of high frequency AC glow discharge has been reported by Munoz et al.<sup>33</sup> to be in the range 120–2000 K and by Yubero et al.<sup>34</sup> to be 800–1900 K. The temperature of dielectric barrier discharge has been reported to be 315–460 K by Lonascut et al.<sup>36</sup> These temperatures reported for a variety of glow discharge plasmas are similar to those measured our rf-GD plasma.

The electron density in our rf-GD was deduced from the Stark broadening of the hydrogen Balmer ( $H_{\beta}$ ) line. A detailed description of the procedure for electron density calculation is given in Section S.2 in the SI. Figure 2(b) shows the electron density plotted as a function of interelectrode distance. The electron density reaches a maximum close to the cathode

surface (negative glow region), and then decrease with the distance from the cathode. This trend agrees well with the prediction of a one-dimensional model of an argon microdischarge.<sup>37</sup> The electron density of our rf-GD system was on the order of  $10^{14} \text{ cm}^{-3}$ , which was consistent with the electron density of similar plasmas reported in the literature.<sup>38–40</sup> However, as expected, electron density induced by glow discharge is lower by 3 to 5 orders of magnitude compared to that in a pulsed spark discharge<sup>4</sup> or laser-induced plasma.<sup>41,42</sup>

### Spatial and temporal distribution of emission signal

We probed the spatial-temporal dynamics of the GD to optimize the signal-to-noise ratio of our rf-GD system. Figures 3(a) and (b) show contour plots of the space-resolved emission spectra, acquired at different locations along the longitudinal axis of the two electrodes in the interelectrode space in the absence of any analyte on the collection electrode. Figure 3 (c) and (d) shows the spectrum obtained at the collection electrode tip (at 0 mm). Several platinum and argon emissions were observed for our rf-GD-OES system. The platinum emission signal from the collection electrode (i.e. cathode) occurs mainly within the 1 mm of the ground electrode surface, with the highest signal appearing at the electrode tip. As expected, the argon emission signal appears across the entire interelectrode gap. These measurements suggest that the excitation of atoms ejected from the cathode, through collisions with ions, electrons, or other atoms in the glow discharge plasma, mainly occur near the cathode surface due to the high density of both negative and positive ions in this region. This observation is consistent with those reported for the solution cathode GD-OES and DC glow discharges at atmospheric pressure.<sup>43–45</sup> The region where platinum emission was observed matches the ‘negative glow’ (NG) region in a typical structure of low-pressure glow discharge. The NG region is the source of light used in GD-OES and allows acquiring most analytical information. Figure 3 (c) and (d) also show that most emission lines are from the neutral species, most likely due to the relatively low temperature of the glow discharge. Ionic emissions can be observed in GD for some elements with low ionization energies, but have been reported to be relatively weak.<sup>23</sup> GD-OES provides fewer emission lines compared to LIBS and spark microplasma emission spectroscopy. In addition, the linewidths are narrower and molecular band emissions are limited. These factors can potentially lower the possibility of spectral interferences.<sup>46</sup>

The temporal characteristics of analyte signal were investigated by acquiring time-resolved spectra with sucrose particles deposited on the collection electrode. Because glow discharge is a continuous plasma, during which the analyte is ablated layer by layer, the analyte signal is a function of time. Figure 4(a) shows the color contour plot for the time-resolved spectra obtained after the glow discharge was initiated (at  $t=0$ , with a gate width of 0.5 s). Figure 4 (b) and (c) shows the spectra obtained at  $t=0$  s and  $t=4$  s, respectively. The carbon emission signal (C I 247.9 nm) is highest at  $t=0$  s and then decreases with time, whereas the platinum emission signals (Pt I 262.8 nm and Pt I 265.9 nm) appear at 0.5 s and then increase with time. At  $t=2$  s, the carbon emission signal disappears, and the platinum emission signal reaches a maximum and remains unchanged. The decreasing carbon signal indicates that the sucrose particles were gradually ablated by the glow discharge. The amount of particulate carbon was predetermined to be 81 ng using Eq. (1). It takes approximately two seconds for

complete ablation of the particulate sucrose (81 ng carbon). Figure 5 shows that the spatially resolved spectra acquired in the presence of sucrose particle deposited on the cathode tip. It is seen that the atomic emission from the ablated particles also occurs in the region near the collection electrode. These spatial and temporal characteristics of our rf-GD system were used to optimize the signal-to-noise ratio and operating characteristics.

### Reproducibility of the plasma characteristics

Continuous operation of the glow discharge can lead to localized heating of the collection electrode and/or changes in electrode surface morphology (due to plasma etching), which in turn may affect particle collection characteristics, subsequently affecting the accuracy and precision of analyte signal measurement. To probe these artefacts, we measured the temperature changes on the cathode (in the absence of analyte on the cathode) using a thermocouple probe. Figure 6 shows variation of the temperature as a function of time after the glow discharge was turned on and off. After the glow discharge is initiated, the cathode temperature rapidly increases to approximately 220 °C. After about  $t=20$  s, the temperature approaches the equilibrium value. The increasing electrode temperature is due to the energy transfer from the reactive species in the plasma (ions, electrons, and metastable species) to the electrode surface.<sup>47</sup> The time dependence of the electrode temperature and the maximum temperature are similar to those reported by Kristya on an atmospheric pressure glow discharge in helium.<sup>48</sup> Figure 6 also shows that once the glow discharge is turned off, the electrode temperature drops to room temperature after approximately 30 s from radiative and convective cooling in CAM. This rapid heating and cooling of the electrode assures short collection cycles. We also note that, as shown in another study,<sup>49</sup> the temperature of the collection electrode (below 300 °C) does not affect the particle collection characteristics of the CAM.

We investigated the repeatability of Ar I and Pt I signal during multiple consecutive glow discharge cycles in the absence of any particulate matter on the cathode. Figure 7 shows variation of Ar I and Pt I signals as a function of time. A glow discharge was continuously produced for 2 min during which the optical emission spectra were recorded every 0.5 s. The time intervals between two glow discharge events is 30 s, which allows the electrode temperature to drop below room temperature. As shown in Figure 7, no discernible variation was observed for the Ar I signal during three subsequent glow discharge cycles (the relative standard deviation was 1.2% for Ar I). However, the signal intensity of the Pt I line increases with time during each glow discharge cycle. This could probably be attributed to the increased cathodic sputtering yield resulting from the thermal effects during the glow discharge.<sup>19,50</sup> The specific lifetime of the electrodes was not determined in this study. The same set of corona and collection electrodes were used for the entire study. No obvious erosion or morphological changes to the electrode surface were noted after more than 100 measurement cycles.

### Analytical performance

Calibration curves for different analytes were constructed by depositing a known particulate mass on the collection electrode, followed by measurement of emission signal as a function of time as described earlier. Figure 8 shows change of cumulative carbon emission signal (C

I 247.9 nm) as a function of time for different particulate loadings. The particulate mass on the electrode tip was varied by changing the collection time, which varied from 1 to 5 minutes. The cumulative carbon emission signal increases with time (and reaches a maximum and remains unchanged after several seconds), indicating that the particles collected on the electrode tip were continuously and completely ablated by the glow discharge. From Figure 8, the time duration required for the complete ablation of the collected particulate carbon, total mass ranging from 16 ng to 81 ng, was approximately 2 seconds.

The time-dependent signal intensity  $I(t)$  of analyte from the glow discharge was integrated to obtain the total emission signal  $I_{tot}$ , such that  $I_{tot} = \int_0^T I(t) dt$ , where  $T$  is the period for which the glow discharge was turned on. Therefore  $I_{tot}$  is the cumulative signal at time  $t$ . Using the data in Figure 8, a calibration curve was constructed by plotting the integrated signal intensity  $I$  as a function of elemental mass ( $m_p$ ) deposited on the electrode tip. Figure 9 shows representative calibration curves for C, Cd, Mn and Na. The selected analytical emission line for each element was C I 247.8 nm, Cd I 508.6 nm, Mn I 403.1 nm, and Na I 589.0 nm. Calibration curves were described using a linear fit. Three sets of measurements were performed for each mass loading. Each data point on the calibration curve represents the average over three replicates. The error bar represents the standard deviation around the mean, and the relative standard deviation, which indicates the reproducibility of spectral response for a given analyte mass, varied in the range of 5 – 28% for all the elements. The inset table in Figure 9 shows that the slope of the log-log plot for all the elements is close to 1, implying a linear relationship between the signal intensity and the elemental mass.

The overall repeatability of our system was comparable to reported values using LIBS techniques that use a similar particle preconcentration method.<sup>9</sup> The uncertainty in the calibration process is from three sources: i) repeatability of spatial and temporal characteristics of the plasma in the interelectrode space, ii) uncertainty in optical emission measurement, and iii) uncertainty associated with the estimation of an analyte mass deposited on the electrode tip. As has been noted elsewhere, other key sources, such as variation in particle size, particle number concentration and collection efficiency fluctuation, are important for accurate mass estimation.<sup>9</sup> The uncertainty is approximately 8.7% for the DMA classified particle diameter, 1% for the particle number concentration, and 1.6% for the collection efficiency. The total estimated uncertainty for the particulate mass is 15%.

The limit of detection (LOD) was estimated using 3- $\sigma$  criteria defined by the International Union of Pure and Applied Chemistry (IUPAC) as,<sup>51</sup>

$$\text{LOD} = 3\sigma / S \quad (3)$$

where  $\sigma$  is the standard deviation of the blank at the selected spectral region and  $S$  is the sensitivity given by the slope of the calibration curve. Blank measurement was obtained in the absence of any particulate mass on the electrode using identical signal collection and spectral processing algorithm. The standard deviation of the blank was obtained by averaging over 15 replicate blank measurements for the spectral region corresponding to



each elemental emission line. The mass LOD was in the range of 0.55 – 1.0 ng depending on elements analyzed, as listed in Table 2. The LOD in terms of air concentration was 7 to 134 ng m<sup>-3</sup> at a flow rate of 1.5 l min<sup>-1</sup> for a sampling time of 5 minutes. A much lower LOD can be achieved by either increasing sampling time or flow rate. The occupational or permissible exposure limits for Cd, Mn, and CNTs are shown in Table 2. It is worth noting that these limits are for 8-hour time-weighted average exposure. Whereas, the LODs from our method are for 5 min sampling time. Even at a 5-min sampling time, the LODs from our method are significantly below the exposure limits. This shows that our method is very sensitive and can readily address routine compliance exposure measurement needs. Table 2 shows the comparison of LODs resulted from different aerosol measurement methods using microplasma spectroscopy, such as GD-OES, LIBS, and SES. The LODs of our rf-GD-OES method coupled with CAM were significantly better than those from particle beam interface GD-OES reported earlier.<sup>25</sup> Also LODs in this study were comparable to those for the LIBS and spark microplasma system coupled with a corona microconcentration system.<sup>4,9</sup> It is worth noting that the detector used in our study was an ICCD, which provides tenfold signal sensitivity compared to the CCD spectrometer used in our earlier studies.<sup>4,9</sup> The LODs of our rf-GD-OES method are higher than those from the other microplasma techniques such as LIBS<sup>9</sup> or SES<sup>4</sup> when using identical optical detection system. However, rf-GD-OES system used in this study has unique advantages with respect to the other techniques. The cost, size, and weight of the excitation source used to produce rf-GD is drastically lower compared to those of other microplasma techniques. This makes the rf-GD-OES methods suitable for developing low-cost monitors for aerosol elemental measurement.

## CONCLUSION

The CAM method for aerosol sampling has been effectively coupled with atmospheric glow discharge optical emission spectroscopy to allow near real-time measurements of elemental concentration of aerosols. The coaxial electrode system in CAM is inherently well-suited for continued particle collection and rf-GD generation. The spatio-temporal dynamics of the rf-GD in CAM were probed to optimize the signal-to-noise ratio for elemental measurement. Artefacts from electrode heating and electrode surface sputtering were negligible and did not interfere with elemental measurement. Calibration curves were obtained by measuring the cumulative emission signal as a function of time for a given elemental mass deposited on the electrode tip. For elements studied in this work (C, Cd, Mn and Na), our method provides detection limits in the range of 7 – 134 ng m<sup>-3</sup> at a flow rate of 1.5 l min<sup>-1</sup> for a 5 minute sampling period. The reproducibility of spectral response was in the range of 5 – 28%. Several other elements, though not studied in this work, can be measured using this system. The near real-time approach developed in this work offers an excellent alternative to development of low-cost, hand-held spectrometers for elemental analysis of aerosols. The method can be implemented on a microfabricated platforms, allowing development of miniature sensors for environmental and occupational health measurement applications.

## Supplementary Material

Refer to Web version on PubMed Central for supplementary material.

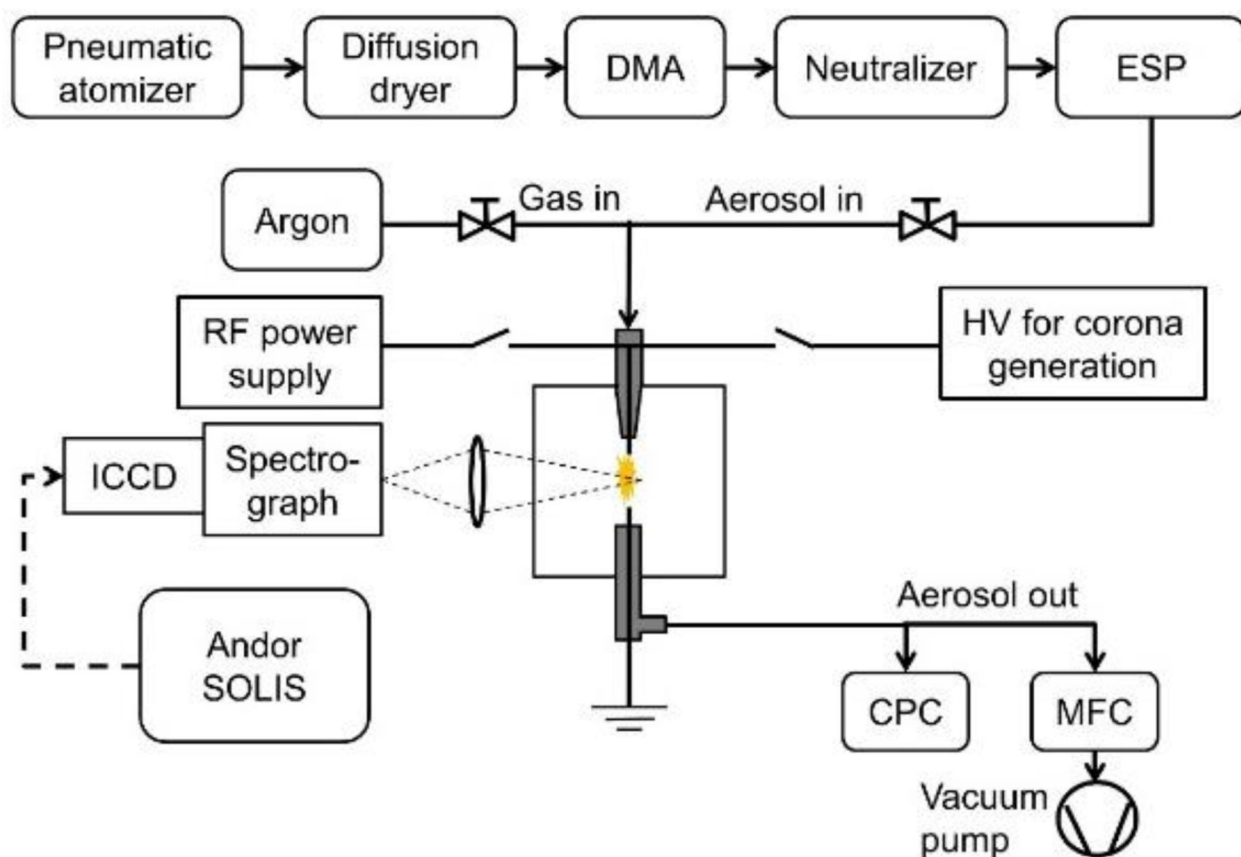
## Acknowledgments

This research work was supported by the NIOSH intramural NORA grant. The authors thank Gregory Deye for his help with the experiments. Authors thank Drs. Amos Doepke and Kevin Ashley for valuable feedback on this manuscript.

## References

1. Pöschl U. *Angew. Chem., Int. Ed.* 2005; 44:7520–7540.
2. Spurny, KR. *Analytical Chemistry of Aerosols: Science and Technology.* CRC; Boca Raton, FL: 1999.
3. Solomon, PA., Fraser, MP., Herckes, P. *Methods for Chemical Analysis of Atmospheric Aerosols.* In: Kulkarni, P., Baron, PA., Willeke, K., editors. *Aerosol Measurement: Principles, Techniques, and Applications.* John Wiley & Sons; Hoboken, NJ: 2011. p. 153-177.
4. Diwakar PK, Kulkarni P. *J. Anal. At. Spectrom.* 2012; 27:1101–1109. [PubMed: 26491209]
5. Hunter AJR, Davis SJ, Piper LG, Holtzclaw KW, Fraser ME. *Appl. Spectrosc.* 2000; 54:575–582.
6. Hunter AJR, Morency JR, Senior CL, Davis SJ, Fraser ME. *J. Air Waste Manage. Assoc.* 2000; 50:111–117.
7. Khalaji M, Roshanzadeh B, Mansoori A, Taefi N, Tavassoli SH. *Opt. Lasers Eng.* 2012; 50:110–113.
8. Park K, Cho G, Kwak J-H. *Aerosol Sci. Technol.* 2009; 43:375–386.
9. Diwakar P, Kulkarni P, Birch ME. *Aerosol Sci. Technol.* 2012; 46:316–332. [PubMed: 26692632]
10. Vors E, Salmon L. *Anal. Bioanal. Chem.* 2006; 385:281–286. [PubMed: 16479369]
11. Radziemski LJ, Loree TR, Cremers DA, Hoffman NM. *Anal. Chem.* 1983; 55:1246–1252.
12. Duan Y, Su Y, Jin Z, Abeln SP. *Anal. Chem.* 2000; 72:1672–1679. [PubMed: 10763268]
13. Kulkarni, P., Efthimion, P. (US DHHS, CDC). *Electrode-assisted microwave-induced plasma spectroscopy.* US Patent 9091597. 2015.
14. Marcus, RK. *Glow Discharge Plasmas as Tunable Sources for Elemental Speciation.* In: Heumann, KG., editor. *Handbook of Elemental Speciation: Techniques and Methodology.* John Wiley & Sons; Chichester, England: 2003. p. 334-355.
15. Jakubowski N, Stuewer D, Vieth W. *Anal. Chem.* 1987; 59:1825–1830.
16. Boumans P. *Anal. Chem.* 1972; 44:1219–1228.
17. Jakubowski N, Dorka R, Steers E, Tempez A. *J. Anal. At. Spectrom.* 2007; 22:722–735.
18. Bengtson A. *Spectrochim. Acta, Part B.* 1994; 49:411–429.
19. Marcus, RK. *Glow discharge spectroscopies.* Springer Science & Business Media; New York: 1993. p. 17-66.
20. Cserfalvi T, Mezei P, Apai P. *J. Phys. D: Appl. Phys.* 1993; 26:2184–2188.
21. Quarles CD Jr, Gonzalez J, Choi I, Ruiz J, Mao X, Marcus RK, Russo RE. *Spectrochim. Acta, Part B.* 2012; 76:190–196.
22. Doroski TA, Webb MR. *Spectrochim. Acta, Part B.* 2013; 88:40–45.
23. Doroski TA, King AM, Fritz MP, Webb MR. *J. Anal. At. Spectrom.* 2013; 28:1090–1095.
24. Wang Z, Schwartz AJ, Ray SJ, Hieftje GM. *J. Anal. At. Spectrom.* 2013; 28:234–240.
25. Marcus RK, Dempster MA, Gibeau TE, Reynolds EM. *Anal. Chem.* 1999; 71:3061–3069. [PubMed: 21662898]
26. Zheng L, Kulkarni P, Zavvos K, Liang H, Birch ME, Dionysiou DD. *J. Aerosol Sci.* 2016; 104:66–78.
27. Karanassios V, Johnson K, Smith AT. *Anal. Bioanal. Chem.* 2007; 388:1595–1604. [PubMed: 17426962]
28. Weagant S, Chen V, Karanassios V. *Anal. Bioanal. Chem.* 2011; 401:2865–2880. [PubMed: 21909664]
29. Weagant S, Karanassios V. *Anal. Bioanal. Chem.* 2009; 395:577–589. [PubMed: 19609509]
30. Obradovic BM, Kuraica MM. *Appl. Phys. Lett.* 2006:89.

31. Winter J, Lange H, Golubovskii YB. *J. Phys. D: Appl. Phys.* 2008; 41:1–6.
32. Revel I, Pitchford LC, Boeuf JP. *J. Appl. Phys.* 2000; 88:2234–2239.
33. Munoz J, Dimitrijevic MS, Yubero C, Calzada MD. *Spectrochim. Acta, Part B.* 2009; 64:167–172.
34. Yubero C, Garcia MC, Varo M, Martinez P. *Spectrochim. Acta, Part B.* 2013; 90:61–67.
35. Yalin AP, Ionikh YZ, Miles RB. *Appl. Opt.* 2002; 41:3753–3762. [PubMed: 12078703]
36. Ionascut-Nedelcescu A, Carlone C, Kogelschatz U, Gravelle DV, Boulos MI. *J. Appl. Phys.* 2008; 103 063305(1-9).
37. Wang, Q. Ph.D. Thesis. University of Huston; Huston, TX: 2006. Plasma diagnostics and modeling of direct current microplasma discharges at atmospheric pressure.
38. Zhou Y-J, Yuan Q-H, Li F, Wang X-M, Yin G-Q, Dong C-Z. *Phys. Plasmas.* 2013; 20 113502(1-6).
39. Belostotskiy SG, Ouk T, Donnelly VM, Economou DJ, Sadeghi N. *J. Appl. Phys.* 2010; 107 053305(1-7).
40. Qian M, Ren C, Wang D, Zhang J, Wei G. *J. Appl. Phys.* 2010; 107 063303(1-5).
41. Dong M, Mao X, Gonzalez JJ, Lu J, Russo RE. *J. Anal. At. Spectrom.* 2012; 27:2066–2075.
42. Harilal SS, Bindhu CV, Nampoori VPN, Vallabhan CPG. *Appl. Spectrosc.* 1998; 52:449–455.
43. Jiang W, Tang J, Wang Y, Zhao W, Duan Y. *Sci. Rep.* 2014; 4 6323(1-6).
44. Staack D, Farouk B, Gutsol A, Fridman A. *Plasma Sources Sci. Technol.* 2005; 14:700–711.
45. Davis WC, Marcus RK. *J. Anal. At. Spectrom.* 2001; 16:931–937.
46. Marcus, RK., Broekaert, J. *Glow Discharge Plasmas in Analytical Spectroscopy.* John Wiley & Sons: Chichester; England: 2003. p. 15-67.
47. Thomann AL, Semmar N, Dussart R, Mathias J, Lang V. *Rev. Sci. Instrum.* 2006; 77 033501(1-6).
48. Kristya VI. *J. Surf. Invest.: X-Ray, Synchrotron Neutron Tech.* 2012; 6:255–258.
49. Zheng L, Kulkarni P, Birch ME, Deye G, Dionysiou DD. *Aerosol Sci. Technol.* 2016; 50:1155–1166. [PubMed: 28638174]
50. Nelson RS. *Philos. Mag.* 1965; 11:291–302.
51. Boumans P. *Anal. Chem.* 1994; 66:A459–A467.
52. NIOSH. *Current Intelligence Bulletin 65: Occupational Exposure to Carbon Nanotubes and Nanofibers.* DHHS NIOSH Publication No. 2013-145; Washington DC: 2013.
53. OSHA. *Regulations (Standards - 29 CFR) PART 1910 Occupational Safety and Health Standards.* Washington DC:



DMA: Differential Mobility Analyzer  
 HV: High Voltage  
 RF: Radio Frequency  
 MFC: Mass Flow Controller

ESP: Electrostatic Precipitator  
 CPC: Condensation Particle Counter  
 ICCD: Intensitified Charge-coupled Device

**Figure 1.**  
 The schematic diagram of the experimental setup.

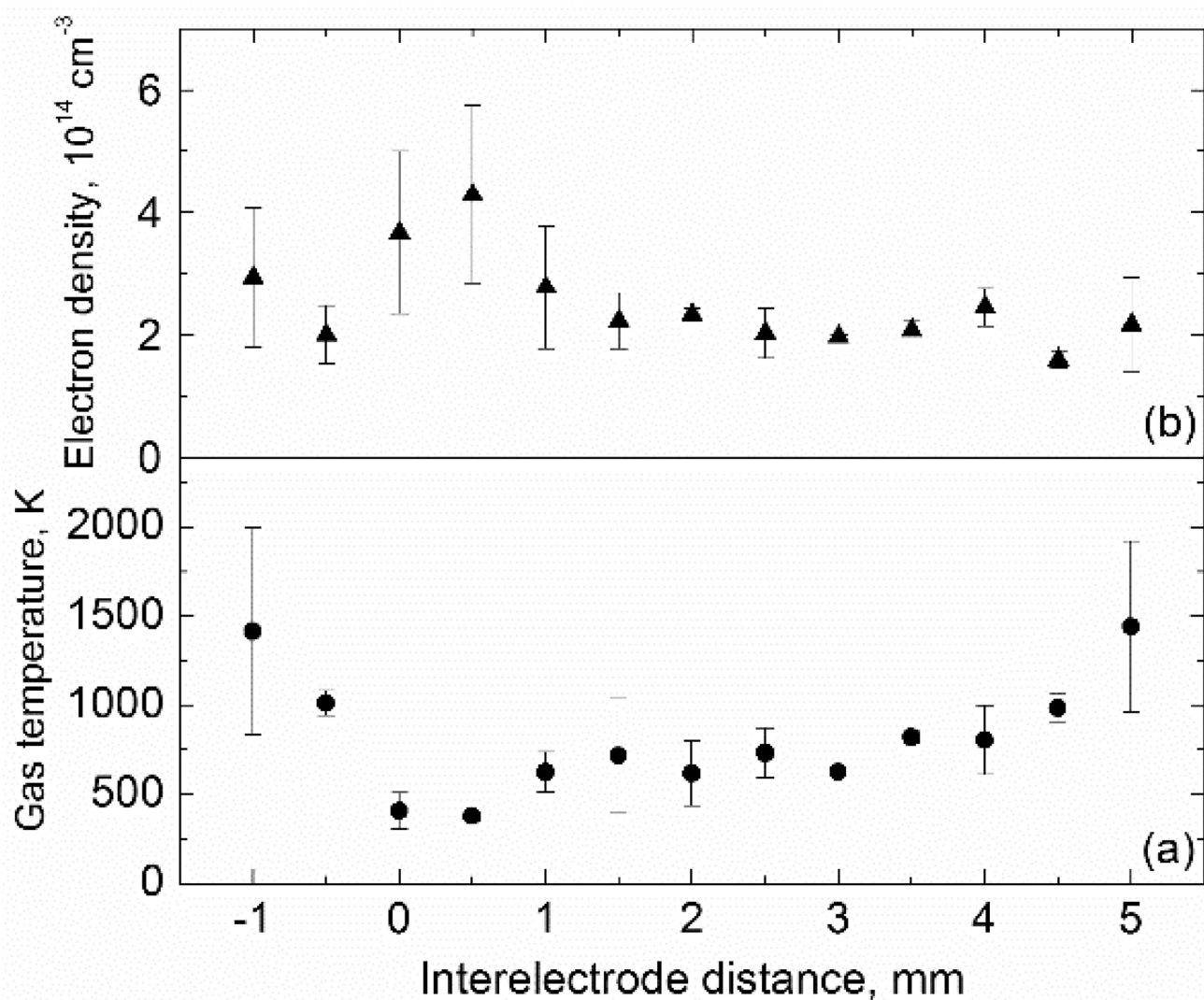


**Figure 2.** The variation of gas temperature (a) and electron density (b) as a function of interelectrode distance. The cathode surface is at 0 mm and the anode surface is at 4 mm.

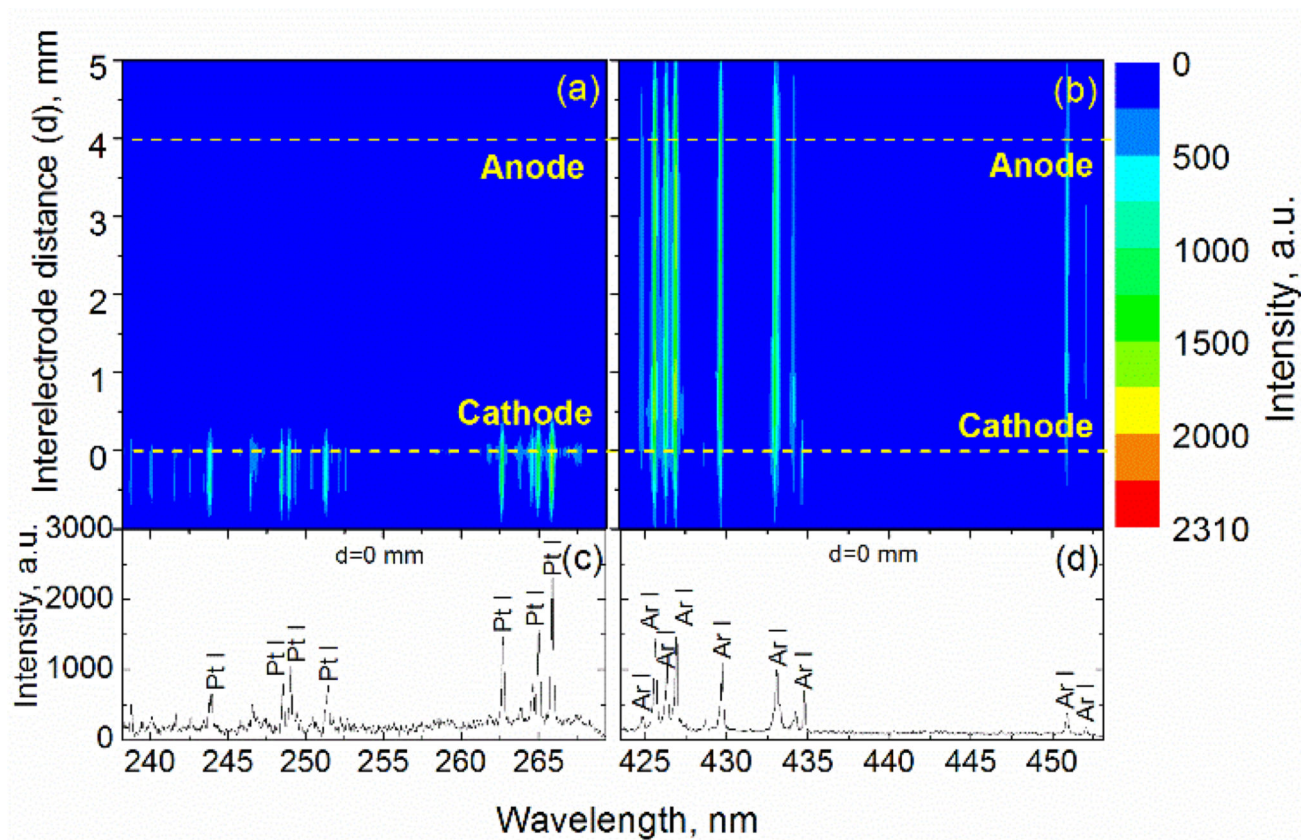


**Figure 3.**

(a) and (b): Spatially resolved rf-GD-OES spectra acquired along the axis of the glow discharge plasma in the absence of analyte on the collection electrode; (c) and (d): corresponding spectrum acquired at the collection electrode tip ( $d = 0$  mm).

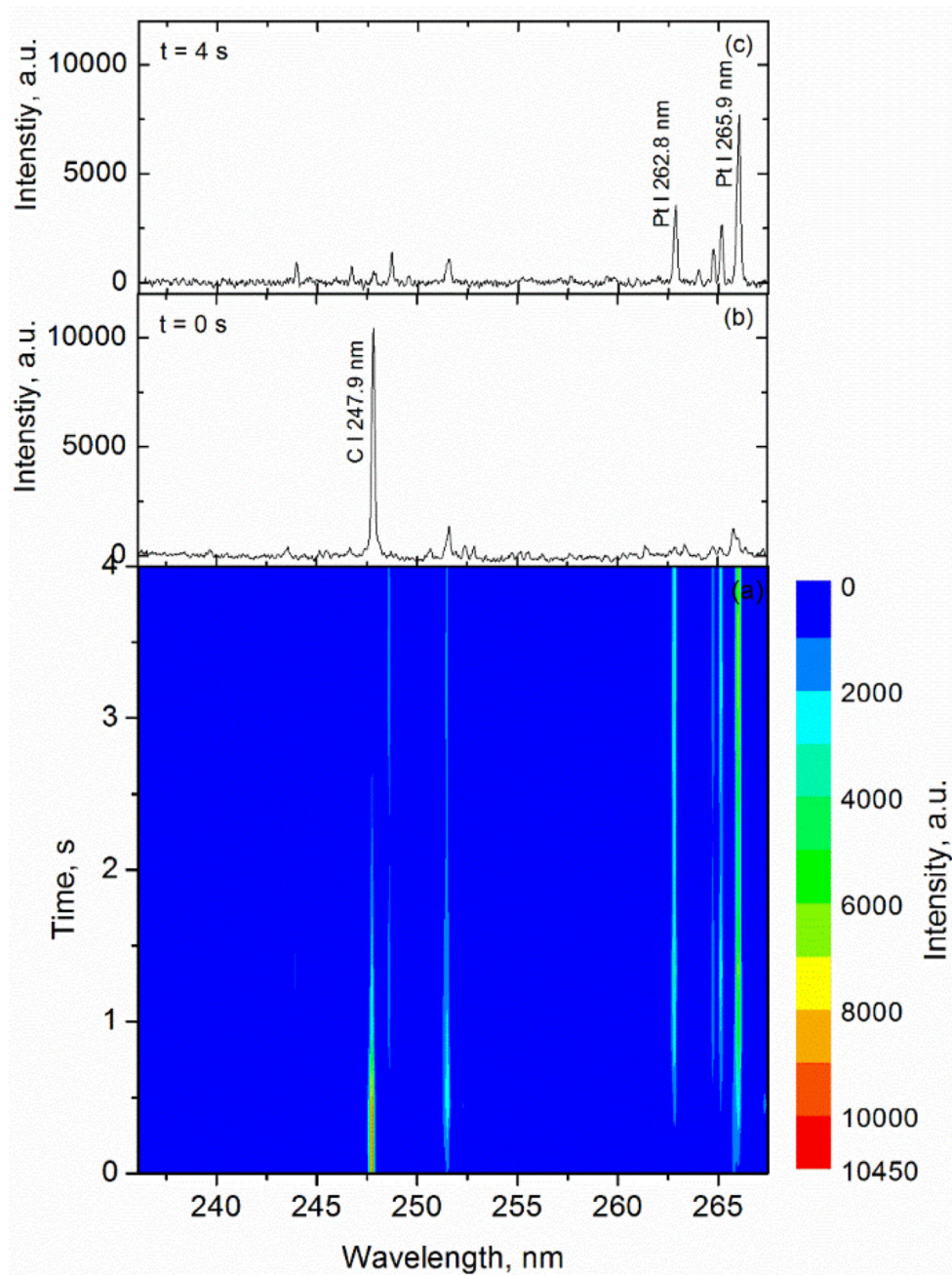


**Figure 4.**

(a) Time-resolved rf-GD-OES spectra acquired between 0 – 4 s after the glow discharge was initiated in the presence of sucrose particles on the collection electrode tip, (b) the spectrum acquired at t=0 s, and (c) the spectrum acquired at t=4 s.

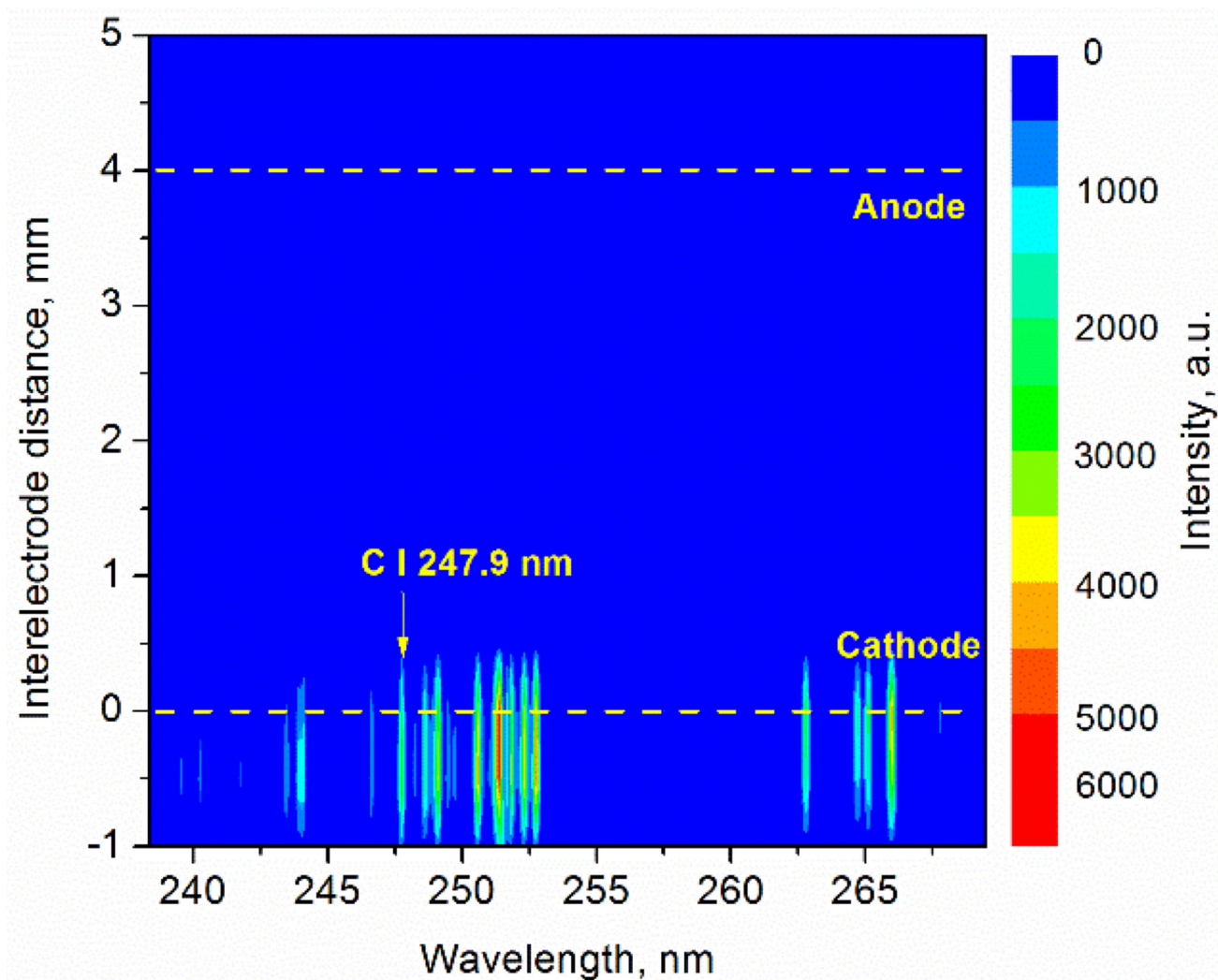


**Figure 5.** Spatially resolved rf-GD-OES spectra acquired along the axis of the glow discharge plasma in the presence of sucrose particles on the collection electrode.



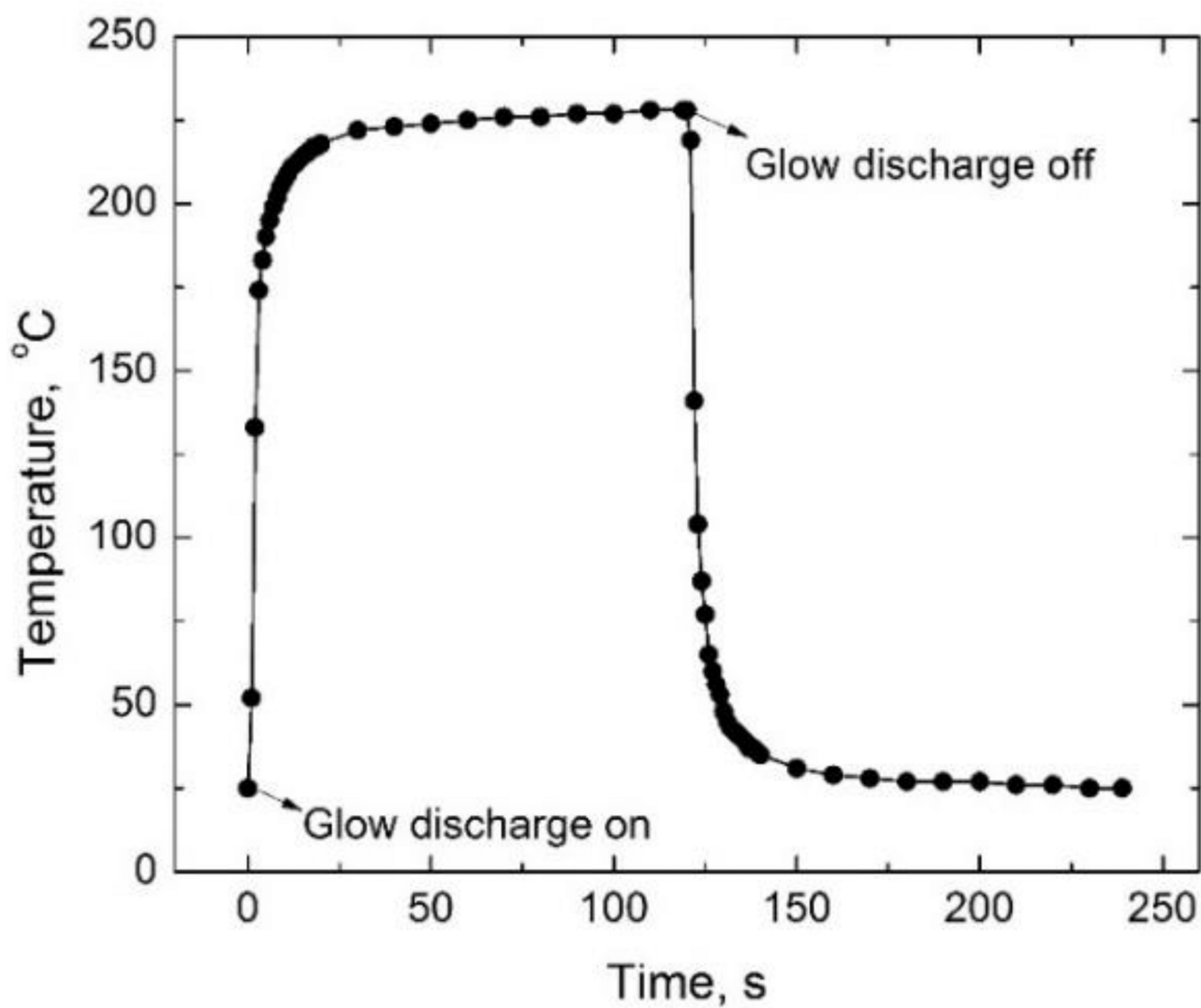


**Figure 6.** Change in temperature at the electrode tip with time when glow discharge on and off (the glow discharge is on at  $t=1$  s and off at  $t=120$  s).

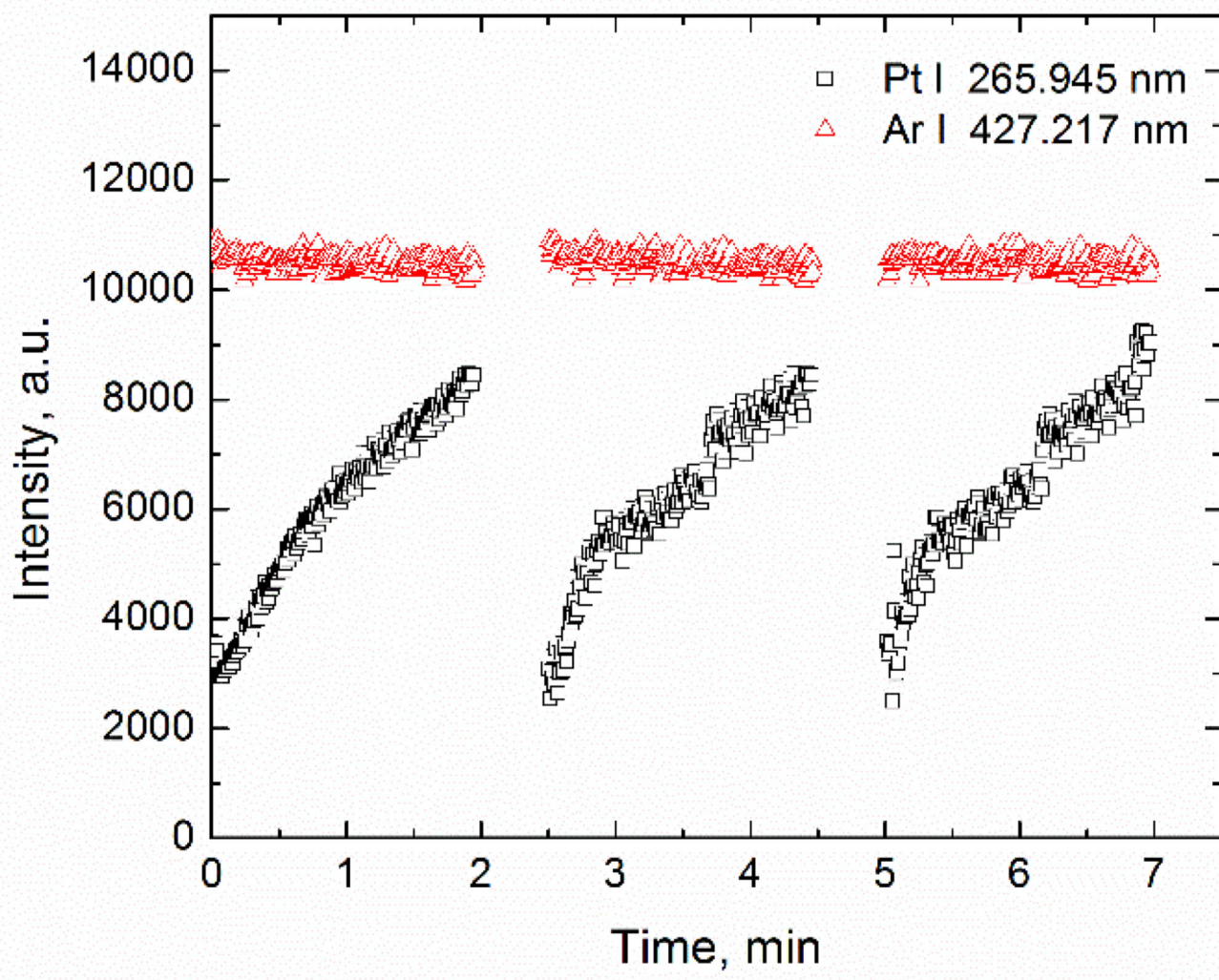


**Figure 7.** Variation of Ar I and Pt I signal intensity as a function of time during consecutive glow discharge cycles.

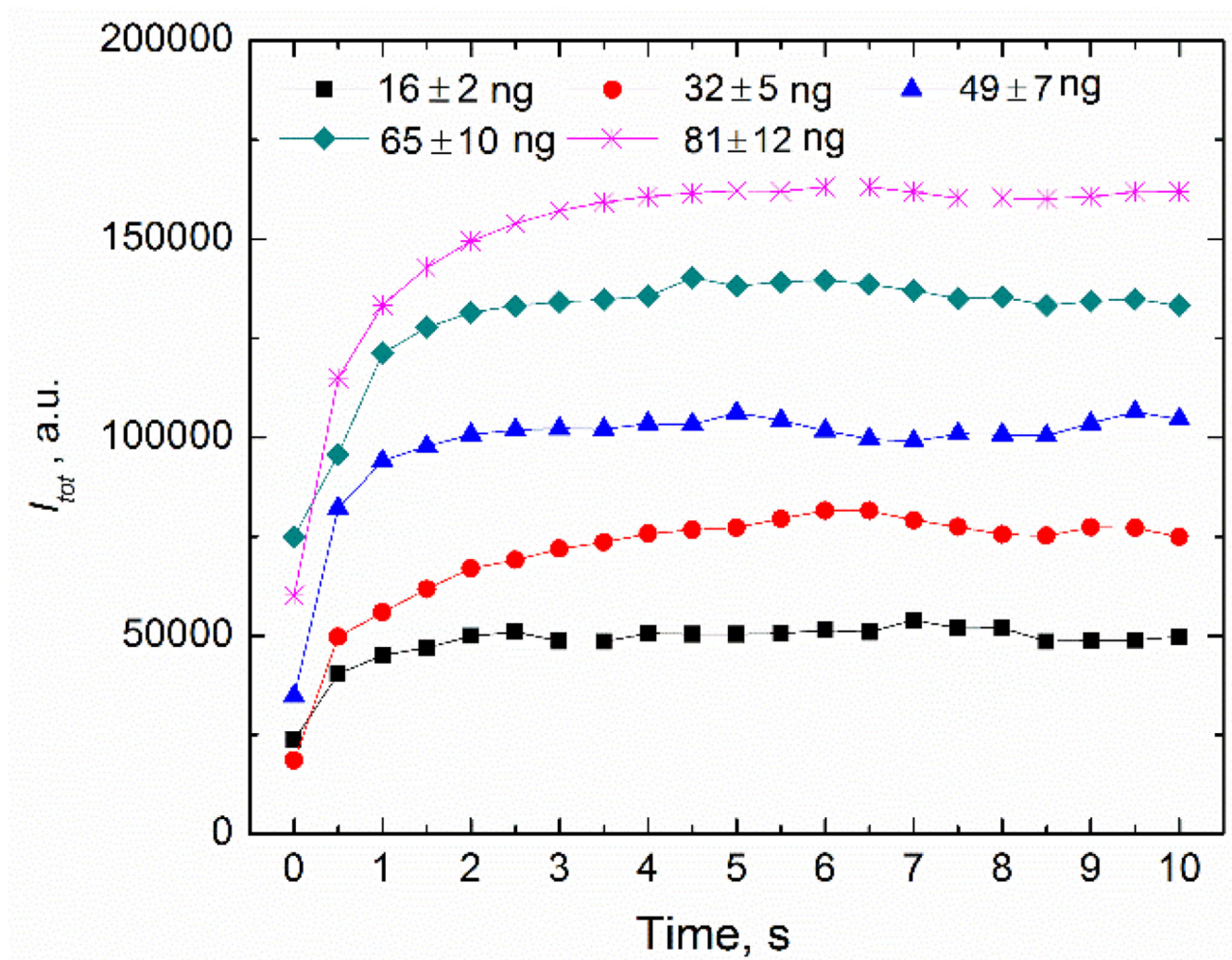


**Figure 8.** Change of analyte signal (C I 247.9 nm) as a function of time for different particulate carbon mass loadings.

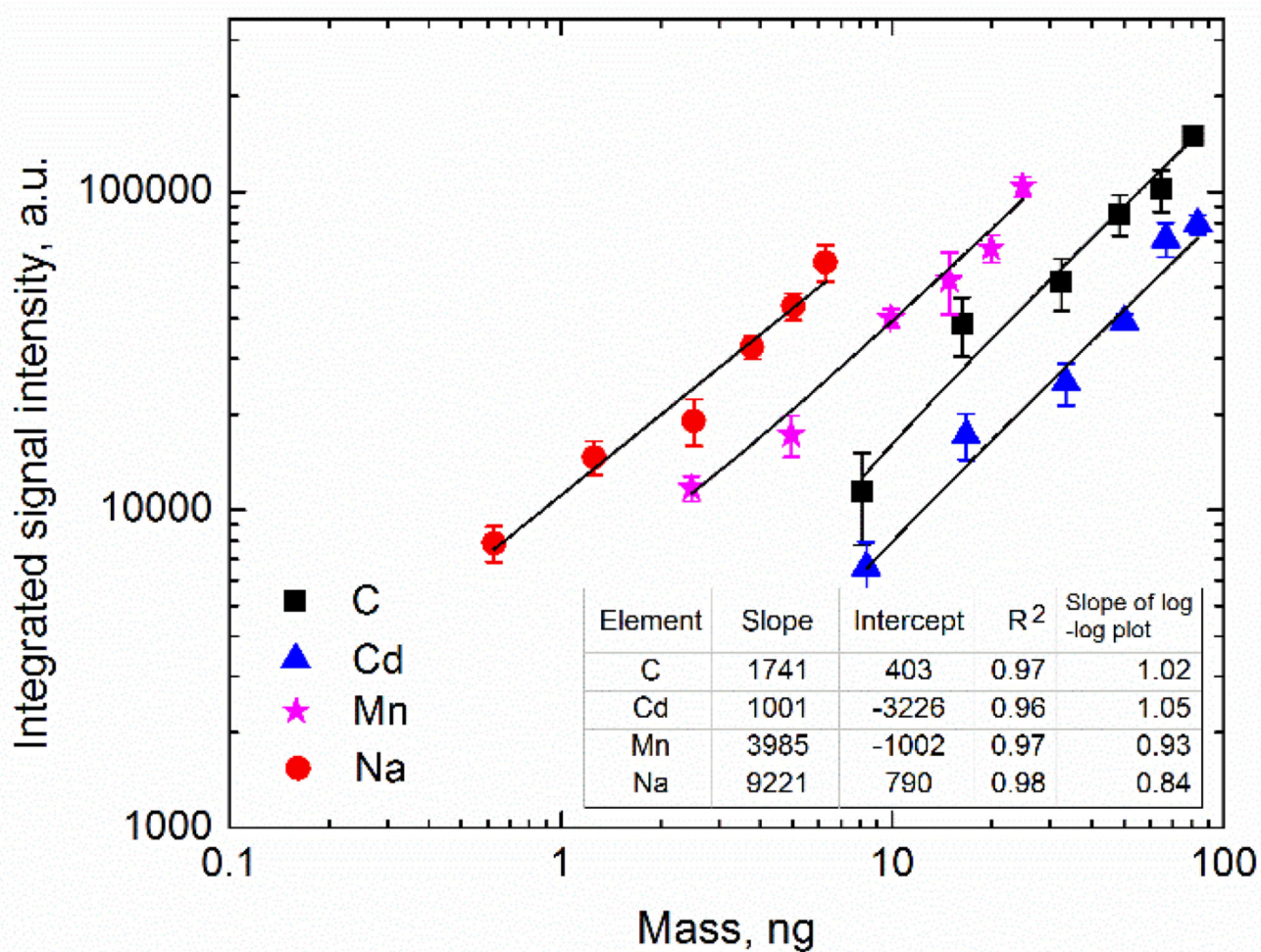


**Figure 9.**  
Calibration curves for C, Cd, Na and Mn obtained using the rf-GD-OES system.

**Table 1**

Materials used to generate calibration aerosol for elements studied in this work.

Element	Source	Chemical composition	Density, g/cm <sup>3</sup>	Mass fraction, %
C	Sucrose solution (Fisher Chemical)	C <sub>12</sub> H <sub>22</sub> O <sub>11</sub>	1.58	42
Cd	Elemental standard solution (Inorganic Ventures)	Cd(NO <sub>3</sub> ) <sub>2</sub>	3.6	47
Mn	Elemental standard solution (Inorganic Ventures)	Mn(NO <sub>3</sub> ) <sub>2</sub>	1.54	30
Na	Sodium carbonate solution (Fisher Chemical)	Na <sub>2</sub> CO <sub>3</sub>	2.54	11

Comparison of mass LODs for various elements (in ng) obtained in this work with those from other microplasma spectroscopy methods

**Table 2**

Elements	GD-OES using CAM (this work)	GD-OES particle beam interface <sup>25</sup>	LIBS using CAM <sup>6</sup>	SES using CAM <sup>4</sup>	Exposure Limits
C	0.49 (65) <sup>*</sup>	--	--	--	1 $\mu\text{g m}^{-3}$ <sup>52</sup> †
Cd	1 (134)	--	5.03 (670)	--	5 $\mu\text{g m}^{-3}$ <sup>53</sup> †
Fe	--	200 (N/A)	--	--	
Mn	0.28 (36)	--	0.155 (20)	--	5,000 $\mu\text{g m}^{-3}$ <sup>53</sup> †
Na	0.055 (7)	30 (N/A)	0.018 (2.4)	0.028 (3.7)	--
V	--	22 (N/A)	--	--	

<sup>\*</sup> Numbers in parenthesis indicate LOD in terms of air concentration in  $\text{ng m}^{-3}$  assuming a collection time of 5 minutes and a flow rate of  $1.5 \text{ l min}^{-1}$

<sup>†</sup> Recommended occupational exposure limit for carbon nanotubes (CNTs) and carbon nanofibers (CNFs) proposed by National Institute for Occupational Safety and Health (NIOSH)<sup>52</sup>

<sup>‡</sup> Permissible exposure limits provided by Occupational Safety and Health Administration (OSHA)<sup>53</sup>